

This is the accepted manuscript made available via CHORUS. The article has been published as:

## Observations of the Effect of Ionization-Potential Depression in Hot Dense Plasma

D. J. Hoarty, P. Allan, S. F. James, C. R. D. Brown, L. M. R. Hobbs, M. P. Hill, J. W. O. Harris, J. Morton, M. G. Brookes, R. Shepherd, J. Dunn, H. Chen, E. Von Marley, P. Beiersdorfer, H. K. Chung, R. W. Lee, G. Brown, and J. Emig

Phys. Rev. Lett. **110**, 265003 — Published 26 June 2013

DOI: [10.1103/PhysRevLett.110.265003](https://doi.org/10.1103/PhysRevLett.110.265003)

## Observations of the effect of ionization potential depression in hot, dense plasma

D. J. Hoarty<sup>1</sup>, P. Allan<sup>1</sup>, S. F. James<sup>1</sup>, C. R. D. Brown<sup>1</sup>, L. M. R. Hobbs<sup>1</sup>, M. P. Hill<sup>1</sup>, J. W. O Harris, J. Morton<sup>1</sup>, M. G. Brookes<sup>1</sup>, R. Shepherd<sup>2</sup>, J. Dunn<sup>2</sup>, H. Chen<sup>2</sup>, E. Von Marley<sup>2</sup>, P. Beiersdorfer<sup>2</sup>, H. K. Chung<sup>3</sup>, R. W. Lee<sup>4</sup>, G. Brown<sup>3</sup>, J. Emig<sup>3</sup>.

(date received etc)

*1 Directorate of Research and Applied Science, AWE plc, Reading, RG7 4PR, UK.*

*2 Lawrence Livermore National Laboratory, 7000 East Avenue, Livermore, CA 94550, USA*

*3 Nuclear Data Section, Division of Physical and Chemical Sciences, International Atomic Energy Agency, P. O. Box 100, A-1400, Vienna, Austria*

*4 Institute for Material Dynamics at Extreme Conditions, University of California, Berkeley, USA.*

(Dated: January 2013)

The newly commissioned Orion laser system has been used to study dense plasmas created by a combination of short pulse laser heating and compression by laser driven shocks. Thus the plasma density was systematically varied between 1 and 10g/cc by using aluminum samples buried in plastic foils or diamond sheets. The aluminum was heated to electron temperatures between 500eV and 700eV allowing the plasma conditions to be diagnosed by K-shell emission spectroscopy. The K-shell spectra show the effect of the ionization potential depression as a function of density. The data are compared to simulated spectra which account for the change in the ionization potential by the commonly used Stewart and Pyatt prescription and an alternative due to Ecker and Kröll suggested by recent X-ray free-electron laser experiments. The experimental data are in closer agreement with simulations using the model of Stewart and Pyatt.

PACS numbers: 57.57.Kk, 52.62.Rr, 52.25.Jm, 52.50.Jm.

In high density plasmas the field from neighbouring ions and free electrons lowers the electron binding energies in the ions relative to the isolated ion values. Recent developments in X-ray free electron lasers have allowed the effect of ionization potential depression (IPD) to be measured in solid density aluminum. In a set of experiments at the Linac Coherent Light Source (LCLS) [1] edge shifts inferred from  $K_{\alpha}$  fluorescence spectra were found to be in disagreement with the Stewart and Pyatt (SP) [2] IPD model widely used since the 1960s, but were closer to an even earlier IPD model proposed by Ecker and Kröll (EK) [3] as discussed in [1] and [4]. This has important implications for dense plasma physics and in particular for the detailed prediction of dense plasma equation of state and radiative opacity in stellar interiors, inertial confinement fusion research, and planetary interiors where the SP model has been used widely. Ionization potential depression is difficult to measure directly because it is in general indistinguishable from the effect of the line merging of high series spectral lines by Stark broadening [5]. However in the data presented in this work the K shell transitions from  $n=2$  and  $n=3$  initial states can be used to compare IPD models where these models predict the disappearance of lines well before they are subject to broadening sufficient to merge them. In this case there is not an ambiguity between merged bound states and

those which disappear due to IPD. This paper describes a study of the effect of IPD in plasmas heated by short pulse laser induced currents to electron temperatures between 500 and 700eV on a timescale of a picosecond. The experiments were carried out at the newly commissioned Orion laser in the UK [6]. The experiments differ substantially from earlier work [7-10] in that this data presents a study of the effect of IPD at higher energy density with the sample density varied systematically over an order of magnitude between 1-10g/cc. This was possible because of some unique features of the Orion laser system which combines short pulse (picosecond) and long pulse (nanosecond timescale) pulses to compress and heat the sample, and by use of samples buried in plastic foils and diamond sheets. The Orion short pulse laser can operate at second harmonic wavelength which suppresses the pre-pulse inherent in conventional infra-red laser systems and greatly increases energy coupling to the solid target [11] allowing the necessary volume of dense material to be efficiently heated. The contrast measurements carried out so far for second harmonic operation have shown the contrast is  $10^{14}$  up to at least 100ps before the main pulse [12]. The findings of the study are that comparing experimental measurements to spectroscopic simulations using the EK model reveals a clear overestimate of IPD with this model under the experimental conditions, but simulations using with the SP

model of IPD are much closer to experimental observation.

The plastic tamped samples used in the study were aluminum dots 100 $\mu$ m in diameter and 0.15 $\mu$ m thick buried in a CH plastic foil (parylene-N) sandwich of 10 $\mu$ m on one side and 12 $\mu$ m on the other, mounted as described in Ref. 11. The face with 10 $\mu$ m coating was irradiated with beam-line 1 of the Orion short pulse OPCPA laser delivering 100J of 2 $\omega$  light (0.53 $\mu$ m wavelength), converted with a type I KDP crystal, in a pulse-length of 0.5ps FWHM. The focal spot was 50 $\mu$ m giving an irradiance of  $1 \times 10^{19}$ W/cm<sup>2</sup>. Spectra were recorded both time-resolved using an ultrafast X-ray streak camera [11] with picosecond temporal resolution coupled to a convex curved (500mm radius of curvature) CsAP crystal and time integrated using flat and convex curved crystal spectrometers recording onto image plate. The spectral resolution ( $E/\Delta E$ ) was 500 in the time resolved case and 600 time-integrated. The response of the spectrometers was absolutely calibrated in order to provide spectral emissivities using off-line x-ray sources to measure the image plate response and reflectivity as a function of x-ray energy.

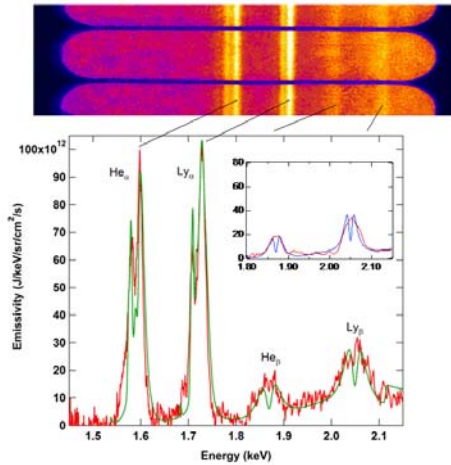


Figure 1: Shock compressed data shown at the top and below a graph of energy vs. emissivity showing a line-out through the experimental time-integrated data (red curve) compared to a synthetic spectrum from FLYCHK (green curve). The inset curve is the time-resolved data recorded on the ultrafast streak camera over the range of the  $n=1-3$  transitions.

The photocathode material used was solid caesium iodide (0.1 $\mu$ m CsI/0.02 $\mu$ m Al/1 $\mu$ m plastic). The X-ray emission source area was measured using an X-ray pinhole array. The time integrating spectrometers were set to record spectra in the range 1.3-2.3keV and the time-resolved spectra were recorded in the range of

1.75-2.2keV as described in Ref 11. When heated by the short pulse laser the thin layer of aluminum expands into the surrounding plastic tamper but the overall foil remains at solid density for around 200ps. The measured x-ray pulse duration is 20ps, consistent with earlier experiments [13] and simulations. The measured spectra are compared to synthetic spectra generated by the FLY [14] and FLYCHK [15] time dependent collisional radiative models, including modelling the pulse duration. The temperature was inferred from the ratio of the  $Ly_{\beta}/He_{\beta}$  emission intensities and the density was inferred from the Stark broadened line-shapes of these emission lines as reported elsewhere [11] and were 600eV and  $1.5 \pm 0.5$ g/cc, respectively.

To provide a controlled density variation, shocks of varied strengths were driven through the foil by irradiating the 12 $\mu$ m side of the foil with two Orion long pulse beams operating in 3 $\omega$  (0.36 $\mu$ m wavelength) in a pulse 0.5ns FWHM with a 140ps rise-time, 200J in each beam and with phase plates giving uniform 300 $\mu$ m focal spots. The beams were synchronized to better than 20ps. The delay between the long pulse beams and the short pulse beam was varied in the experiments.

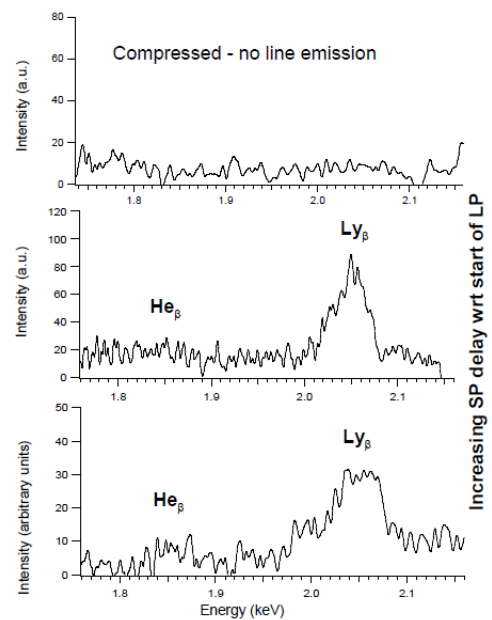


Figure 2: Emission spectra recorded on the streak camera at various times during the shock wave transit through the target. For the bottom and middle curves the shock has not yet arrived at the aluminum layer position. In the top curve the shock has compressed the aluminum and the  $n=3$  levels have become delocalized.

In the time after shock compression of the buried layer but before shock breakout, the short pulse beam irradiates the 10 $\mu$ m plastic face to heat the

compressed tamper and sample. Figure 1 shows the measured spectra from shock compressed aluminum in plastic. The graph shows the experimental emissivity compared to a spectrum predicted by FLYCHK with the predicted emissivity scaled by 1.17. The FLYCHK peak electron temperature was 550eV and the density inferred was 6g/cc. The inset curve shows the  $n=1-3$  transitions measured on the X-ray streak camera on the same laser shot as the time-integrated measurement along with a comparison to FLYCHK. The density inferred was the same as the time-integrated data but the peak electron temperature inferred from the time-resolved data was slightly higher at 600eV. Spectra at intermediate density, 3g/cc and slightly higher peak electron temperature of 700eV, were measured by using samples of aluminum tamped in diamond sheet. The targets were 100 $\mu$ m diameter 0.15 $\mu$ m thick aluminum dots sandwiched in 10 $\mu$ m diamond at 3.5g/cc and 4 $\mu$ m diamond-like carbon at 3g/cc. The laser conditions were identical to the plastic experiments apart from a smaller focal spot on the short pulse beam of 20 $\mu$ m. The diamond tamped aluminum remains at 3g/cc during the X-ray emission pulse. The tamping effect of the diamond is reasonably well modelled by radiation-hydrodynamics simulations using the NYM code [11, 16, 17].

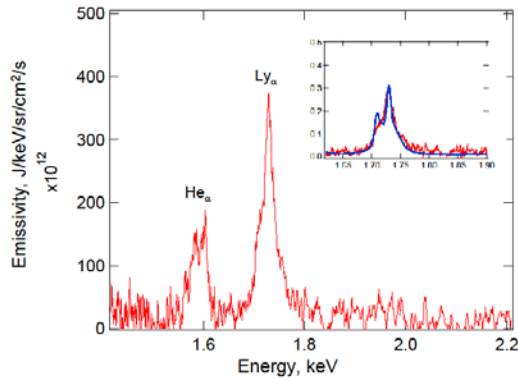


Figure 3: X-ray emission spectra from shock compressed aluminum in diamond. Inset comparison of measured and simulated  $Ly_{\alpha}$  line-shape indicates 9g/cc.

To achieve higher densities the diamond was shocked by one of the long pulse beams of Orion incident on the 10 $\mu$ m diamond face. Figure 2 shows the emission recorded on the X-ray streak camera at different delays during the transit of the shock wave through the diamond target. In the lower two curves the shock wave has not yet arrived at the aluminum dot position, and the  $n=1-3$  transitions from He-like and H-like aluminum ions are clearly visible. The delay

between the onset of the long pulse and the short pulse is 200ps and 260ps respectively. A comparison of the recorded spectra to FLYCHK simulations shows that the temperature is similar to that recorded in the unshocked diamond experiments. In the upper curve the shock has arrived at the aluminum layer and compressed the aluminum. The  $n=3$  transitions are no longer evident in the spectrum because of the delocalization of the  $n=3$  levels in the He-like and H-like ions due to ionization potential depression. In the absence of  $He_{\beta}$  and  $Ly_{\beta}$  lines the conditions for the data in the top curve of Fig. 2 must be inferred from the time-integrated data. The  $Ly_{\alpha}$  line-shape was used to infer the density and the  $He_{\alpha}/Ly_{\alpha}$  ratio was used to estimate the temperature. Though opacity effects at the line center mean that this method is not as accurate as the density and temperature inferred from the optically thin  $n=1-3$  transitions, and there is a discrepancy in the satellite line intensity, a reasonable estimate can be inferred in this case. Fig. 3 shows the time-integrated spectra recorded from shock compressed aluminum in diamond. The  $n=3$  transitions are absent but the  $He_{\alpha}$  and  $Ly_{\alpha}$  lines can be clearly seen. The inset is a comparison of the  $Ly_{\alpha}$  line-shape with the prediction of FLYCHK which indicates a density of  $9 \pm 1$ g/cc.

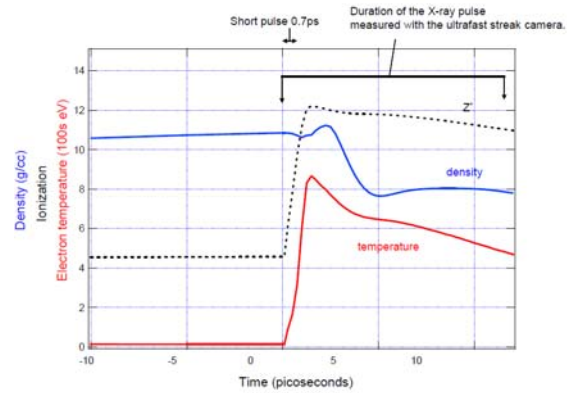


Figure 4: Conditions in the shocked aluminum layer with a diamond tamper predicted by the radiation-hydrodynamics code. The peak electron temperature and density are in reasonable agreement with the conditions inferred from the emission spectrum.

An additional estimate of the density can be taken from the radiation-hydrodynamics simulations of the shocked target. The shock transit time in the experiment was measured which allowed the radiation-hydrodynamics simulations to be benchmarked. To reproduce the measured transit time in the radiation-hydrodynamics simulations the irradiance on target was reduced from the measured value. The

radiation-hydrodynamics predictions for density, temperature and ionization are shown in Fig. 4. The shocked aluminum density reaches just over 10g/cc and drops to 8g/cc during the duration of the X-ray emission recorded on the streak camera. The predicted conditions are in reasonable agreement with those inferred from the spectra. Line-outs of the aluminum spectra measured with the ultrafast streak camera and crystal spectrometer in the range 1.8-2.2keV are shown in Fig. 5. The measurements, at the various densities sampled experimentally, are shown alongside the predictions of the FLYCHK code using both the SP and EK models of IPD, with the same prescription for SP and EK models used here as in Ref 1. The curves of both experiment and simulation are in arbitrary units and have been scaled in intensity for clarity. The experimental curves from bottom to top were fitted at the following conditions of the total aluminum material density and peak electron temperature:  $1.2 \pm 0.4$ g/cc, 550eV;  $2.5 \pm 0.3$ g/cc, 650eV;  $4 \pm 0.5$ g/cc, 700eV;  $5.5 \pm 0.5$ g/cc, 550eV;  $9 \pm 1$ g/cc, 700eV. The simulations use the measured density but the temperature in all cases is 700eV. The simulations using the SP prescription for IPD are in qualitative agreement with experiment but suggest that delocalization of the  $n=3$  levels, from bound states to the continuum, would occur at a slightly higher density (11.6g/cc) than indicated by the experiments. This curve is the top curve of the SP plots in Fig. 5. However the abrupt steps at the bound-free edges in the simulations are unphysical and a more realistic picture should include broadening of the bound-free edges due to fluctuations [18]. In contrast the simulations with the EK model for IPD predict a very different outcome. The EK model predicts delocalization of the  $n=3$  levels at all but the lowest density sampled in the experiment. Importantly the EK model removes the  $n=3$  level to the continuum by IPD at a density too low for Stark broadening of the lines and merging with the continuum to be an alternative possibility according to line-shape theory; theory which has been verified against experiment over several decades [14,19-21]. The densities inferred from Stark broadening of measured spectra are consistent with the radiation-hydrodynamics predictions of the target density. On the experimental timescale the density of the tamper determines the density in the sample because the thickness of the foil or diamond sheet means there is insufficient time for the rarefaction wave

from the outer surface to move inward significantly.

Following the convention in Ref. 18 in the high density limit the shift in ionization potential for SP and EK models can be written as :-

$$\Delta I_{SP}(Z) = \frac{3(Z+1)e^2}{2R_o} \quad (1)$$

and

$$\Delta I_{EK} = \frac{(Z+1)e^2}{R_{EK}} \quad (2)$$

$$\text{where } \frac{4\pi n_i R_o^3}{3} = 1 \quad (3)$$

$$\text{and } R_{EK}^3 = \frac{R_o^3}{1 + \langle N_e \rangle} \quad (4)$$

Here  $n_i$  is the ion number density, and  $\langle N_e \rangle$  is the average number of free electrons per ion. For a highly ionized system  $\Delta I_{EK}$  is larger than  $\Delta I_{SP}$  by the additional scaling  $\langle N_e \rangle^{1/3}$ .

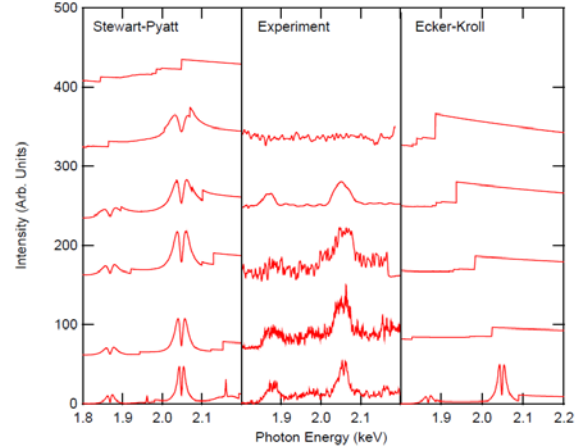


Figure 5: A compilation of the experimental data at different densities compared to FLYCHK predictions using Stewart and Pyatt and Ecker and Kröll treatments of ionization potential depression. The density of the curves from bottom to top is 1.2, 2.5, 4, 5.5 and 9g/cc. The SP plot has an additional curve at 11.6g/cc.

The data in Fig. 5 show that this additional shift is a large overestimate of the effect and that the Stewart and Pyatt model is closer to the experimental measurements in this regime. The data show that  $n=3$  transitions are clearly observed up to densities of at least 6g/cc, indicating that the IPD shift has not delocalized the  $n=3$  levels. The data and radiation-hydrodynamics simulations suggest that at a density between 8 and 10g/cc the  $n=3$  levels are delocalized and that the  $n=1-3$  line transitions disappear from the spectrum. In summary, a systematic study of the effect of IPD on the

delocalization of  $n=3$  levels in aluminum has demonstrated much closer agreement between the measurements and predictions of simulations using the SP model of IPD than with those using the EK model and over the range of the experimental conditions the EK model overestimates the IPD shift significantly. Although the SP model is a simple analytical approximation relying on the semi-classical Thomas-Fermi approximation, the model prediction is close to experiment though some discrepancy remains. The data described will be compared to more sophisticated models in due course. The authors would like to thank the laser and facility staff of the Orion laser; D. Lavender for engineering support and the staff of AWE target fabrication. Work at the Lawrence Livermore National Laboratory was performed under the auspices of the DOE under contract DE-AC52-07NA-27344.

- [1] O. Ciricosta et al, Phys. Rev. Lett. **109**, 065002 (2012)
- [2] J. C. Stewart and K. D. Pyatt, Jr., Astrophys. J. **144**, 1203 (1966)
- [3] G. Ecker and W. Kröll, Phys. Fluids **6**, 62 (1963)
- [4] T. Preston et al, High Energy Density Physics (2013). <http://dx.doi.org/10.1016/j.hedp.2012.12.014>
- [5] D. R. Inglis and E. Teller, Astrophys. J. **90**, 439 (1939)
- [6] N. W. Hopps et al, Proc. of SPIE Vol 7916, 79160C doi :10.1117/12.874252
- [7] D. K. Bradley et al Phys. Rev. Lett. **59**, 2995 (1987)
- [8] D. Riley et al, Europhys. Lett. **10**, 135 (1989)
- [9] M. Nantel et al, Phys. Rev. Lett. **80**, 4442 (1998)
- [10] J. Osterholz et al, Phys. Rev. Lett. **96**, 085002 (2006)
- [11] C. R. D. Brown et al, Phys. Rev. Lett. **106**, 185003 (2011)
- [12] D. Hillier et al, Applied Optics (2013) to be published.
- [13] D. J. Hoarty et al, High Energy Density Physics, **6**, 105 (2010)
- [14] R.W. Lee, J. T. Larsen, JQSRT **56**, 535 (1996)
- [15] H. K. Chung et al, High Energy Density Physics **1**, 3 (2005)
- [16] D. J. Hoarty et al Phys. Plasmas, **6**, 2171 (1999)
- [17] P. D. Roberts et al, Phys. D. **13**, 1957 (1980)
- [18] C. A. Iglesias and P. A. Sterne, High Energy Density Physics, **9**, 103 (2013)
- [19] H. R. Griem, *Principles of Plasma Spectroscopy*, Cambridge University Press (1997)
- [20] H. R. Griem, *Spectral Line Broadening by Plasmas*, Academic Press, New York, (1974)
- [21] H. J. Kunze, *Introduction to Plasma Spectroscopy*, Springer (2009) and references therein.